New Hybrid Model for Evaluating the Frequency-Dependent Leakage Inductance of a Variable Inductance Transformer (VIT)

Angshuman Sharma
Department of Electrical and Computer Engineering
Missouri University of Science and Technology
Rolla, MO USA
asc4v@mst.edu

Jonathan W. Kimball
Department of Electrical and Computer Engineering
Missouri University of Science and Technology
Rolla, MO USA
kimballjw@mst.edu

***Abstract*—Skin and proximity effects can cause a significant drop in the effective leakage inductance of a transformer when the operating frequency is increased. Although the magnetic image method-based double-2-D model can calculate the low-frequency leakage inductance with sufficient accuracy, it is inherently a frequency-independent model. While Dowell's 1-D model uses frequency-dependent relations to account for both skin and proximity effects, its accuracy is severely affected by the assumed winding geometry. In this paper, a hybrid model is proposed that uses superposition to combine a modified Dowell's model with the double-2-D model. The proposed model is investigated on a variable inductance transformer (VIT)—a partially-filled transformer whose leakage inductance can be varied by moving one of the windings mechanically. The frequency-dependent leakage inductances of the VIT evaluated using the hybrid model are in excellent agreement with the corresponding finite element method (FEM) simulated and experimentally measured values, thereby validating the proposed hybrid model.**

***Index Terms*—Double-2-D model, Dowell's 1-D model, hybrid model, leakage inductance, variable inductance transformer.**

I. Introduction

Leakage inductance is a critical design element of a transformer used in a galvanically isolated power electronic converter. In a multi-layered transformer with integrated magnetics, the skin and proximity effects can disturb the homogeneity of the current density across the cross-sections of the conductors. For a given wire gauge, these eddy current effects become more pronounced as the operating frequency of the power converter is increased. Consequently, the leakage inductance seen at a higher frequency can be significantly smaller than that at a lower frequency [1]. Therefore, it is important to determine the leakage inductance at the specific operating frequency range of the transformer, especially in resonant converters with variable frequency control.

The calculation of leakage inductance is inherently a 3-D problem. Numerical techniques to solve this 3-D problem are available in the form of Finite Element Methods (FEM), which are accurate but computationally expensive [2, 3]. On the other hand, multi-objective optimizations of power electronic converters require swift yet accurate calculation methods. Hence, analytical or semi-analytical methods are usually preferred [4, 5]. Such methods can be broadly classified into either 1-D or 2-D models, and either low-frequency (LF) or high-frequency (HF) models. While 1-D models consider only the axial component of magnetic field intensity [6], the 2-D models consider both the axial and the radial components, which makes them an excellent choice for partially-filled transformers. In contrast to LF models, the HF models take into account the eddy current effects in transformer windings, thus making them suitable for HF magnetic designs. A comparison of the existing LF models can be found in [5]. Among the LF models, the magnetic image method-based double-2-D model has drawn a lot of attention lately due to its exceptional adaptability to different winding geometries and core shapes including partially-filled transformers [2, 3, 7, 8, 9, 10, 11, 12].

A 2-D HF model currently does not exist. Dowell pioneered the development of a 1-D model that accounts for the eddy current effects in the windings of fully-filled transformers [13, 14]. The fundamental assumption was that the winding cross-sections are frequency-dependent and non-winding spaces are frequency-independent regions. Inspired by Dowell's work, Hurley [15, 16] and Niemela [17] individually made some remarkable progress in solving the Helmholtz differential equation for the magnetic field intensity inside the winding cross-section of a rectangular foil. To enhance accuracy, Bahmani [18] and Ouyang [19] made some further improvements to Hurley's model. However, all of these models assume that the radial component of magnetic field intensity is zero, and that its axial component depends only on the position of the foil along the radial axis. These drastic simplifications limit the applicability of the existing HF models to fully-filled transformers only that have a winding height comparable to the window height. Although Rogowski's factor or other porosity factors are suggested in [1, 14, 20] for winding heights shorter than window height, the resulting error still increases with the difference between the two heights. Therefore, an HF model that can calculate the frequency-dependent leakage inductance of partially-filled transformers is still missing in literature.

Recently, a variable inductance transformer (VIT) was introduced in [12]. It is a partially-filled transformer that has a winding height significantly smaller than the window height. Fig. 1 shows the 2-D model of a VIT. By moving one of

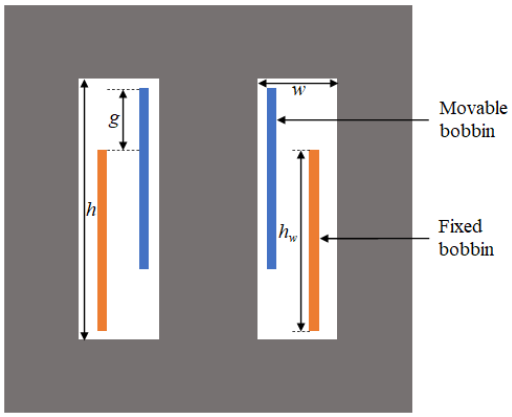

Fig. 1. 2-D model of a VIT.

the bobbins along the core leg, the overlapping height of the two windings ($= h_w - g$) can be reduced. This increases the radial component of magnetic field intensity, leading to a higher leakage inductance. The improved double-2-D model proved very effective in evaluating the variable LF leakage inductance of a VIT in [2].

In this paper, a hybrid model is proposed for evaluating the variable HF leakage inductance of a VIT. The model uses superposition to combine a modified HF Dowell's model with the LF double-2-D model. The paper is arranged as follows. Section II gives a brief outline of the double-2-D model. Section III uses previous results from the double-2-D model to explain the phenomenon of varying leakage inductance in a VIT; also highlighting the shortcomings of the existing HF models. Section IV derives the Dowell's 1-D model from Maxwell's equations. Section V modifies the derived Dowell's model and proposes the new hybrid model. Section VI presents and discusses the results obtained using the proposed model, and section VII finally concludes the paper.

II. Double-2-D Model

Evaluation of leakage inductance is inherently a 3-D problem. The double-2-D model reduces this 3-D problem into two separate 2-D problems, wherein the magnetic energy per unit length E' is evaluated across two planes—the IW plane and the OW plane—using the fundamental equation [2, 12],

$$E' = \frac{\mu_0}{2} \iint H_{\text{2-D}}^2(x, y)\, dx\, dy \tag{1}$$

where μ_0 is the permeability of free space, and $H_{\text{2-D}}$ accounts for both the radial H_x and axial H_y components of magnetic field intensity across the entire plane under consideration, thus making the double-2-D model very promising especially for partially-filled transformers.

Fig. 2 illustrates the concept of the improved double-2-D model [2, 12]. The general form of this model is given by,

$$L_{lk,\text{double-2-D}} = s_c \left(L'_{\text{2-D(IW)}} d_{l(\text{IW})} + L'_{\text{2-D(OW)}} d_{l(\text{OW})} \right) \tag{2}$$

$$s_c = \begin{cases} 1, & \text{core-type transformer} \\ 2, & \text{shell-type transformer} \end{cases}$$

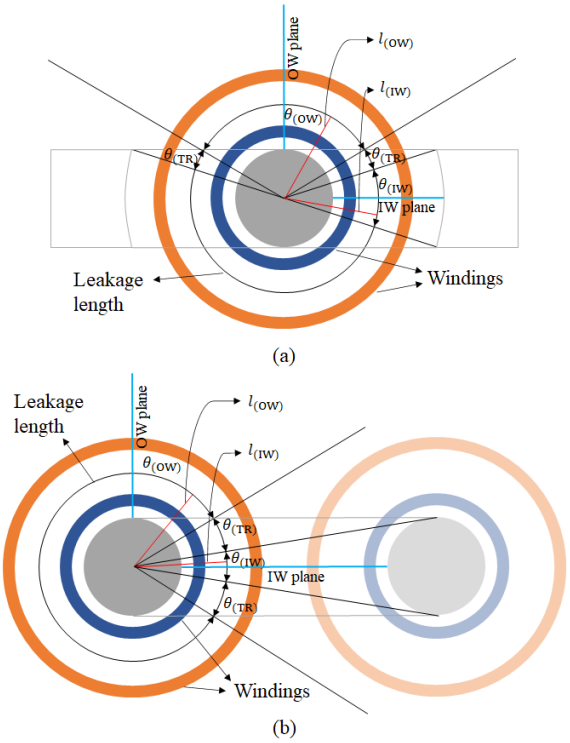

Fig. 2. Double-2-D model: (a) shell-type transformer, (b) core-type transformer. $l_{(\text{IW})}$ and $l_{(\text{OW})}$ are the leakage radii for the IW and OW planes. $\theta_{(\text{IW})}$, $\theta_{(\text{IW})}$ and $\theta_{(\text{TR})}$ are the leakage angles for the IW, OW and transition (TR) regions. Partial leakage lengths are calculated using these parameters in [2].

where $L'_{\text{2-D}}$ is the leakage inductance per unit length across the IW or OW plane, and d_l is the partial leakage length of the IW or OW region. The underlying assumptions are that the leakage inductance per unit length evaluated across a plane is uniform along its leakage length, and the stored magnetic energy inside the core is zero.

To find the leakage inductance per unit length across a plane, the magnetic energy per unit length evaluated using (1) must be scaled by a factor of $2/I_1^2$, where I_1 is the primary current. The improved model averages the magnetic energy per unit length across each plane to find the corresponding leakage radius, which is then used to find the partial leakage length. Finally, the total leakage inductance can be obtained by using (2). The detailed mathematics of the improved double-2-D model can be found in [2, 12].

The double-2-D model uses the magnetic image method to calculate the magnetic energy per unit length across the two planes. As per the image method, the transformer core acts as a reflective medium for any current-carrying conductor placed near it. The IW plane that is bounded by the core on all four sides results in an infinite series of image conductors, while the OW plane that is bounded by the core on one side only results in a single image conductor. Hence, the accuracy of the double-2-D model depends on the number of image layers being considered in the IW plane. Reference [2] suggests that two image layers must be considered at the least for an acceptable accuracy of the evaluated leakage inductance.

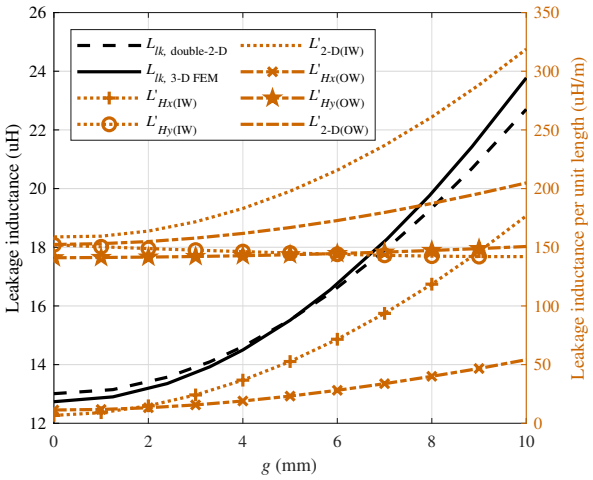

Fig. 3. Plot showing the variable LF leakage inductance of a VIT [2].

III. Variable Inductance Transformer

A VIT is a partially-filled transformer that allows users to vary its leakage inductance mechanically. The improved double-2-D model proved very effective in evaluating the variable LF leakage inductance of a VIT because it: 1) analyzes an OW plane in addition to the IW plane, 2) considers both radial and axial components of magnetic field intensity, 3) accounts for the position of the winding along both $x-$ and $y-$axes, and 4) uses partial leakage lengths as the depths of the planes. Fig. 3 plots the analytical and FEM simulated variable LF leakage inductance as a function of the reduction in overlap g between the two windings. A maximum error of only 4.5 % was noticed at $g = 10$ mm when the nearest three image layers (48 images) were considered in the IW plane [2].

Fig. 3 also plots the variations in L'_{Hx}, L'_{Hy} and $L'_{2\text{-D}}$ with g, where L'_{Hx}, L'_{Hy} and $L'_{2\text{-D}}$ are the LF leakage inductances per unit length across the IW or OW plane considering the radial component of magnetic field intensity H_x, axial component H_y, and their phasor sum $H_{2\text{-D}}$, respectively, so that $L'_{Hx} + L'_{Hy} = L'_{2\text{-D}}$. This figure suggests that an increase in g has a negligible effect on H_y in both planes. Instead, the increase in leakage inductance is an outcome of the increase in H_x only, if partial leakage lengths are assumed constant. Since the existing HF models ignore H_x entirely and fail to account for the position of the winding along the $y-$axis, using such models in a VIT will result in a constant leakage inductance at different overlaps g. Moreover, the increase in L'_{Hx} is seen to be much more across the IW plane than the OW plane so that $L'_{2\text{-D(IW)}} \gg L'_{2\text{-D(OW)}}$ for $g > 0$ mm. Hence, analyzing the IW plane only will overestimate the total leakage inductance. Therefore, a new HF model is desired that analyzes an OW plane besides the IW plane, accounts for the radial component in addition to the axial component at least in the non-winding spaces, and takes into account the true position of the windings along both $x-$ and $y-$axes to compute the variable HF leakage inductance of a VIT.

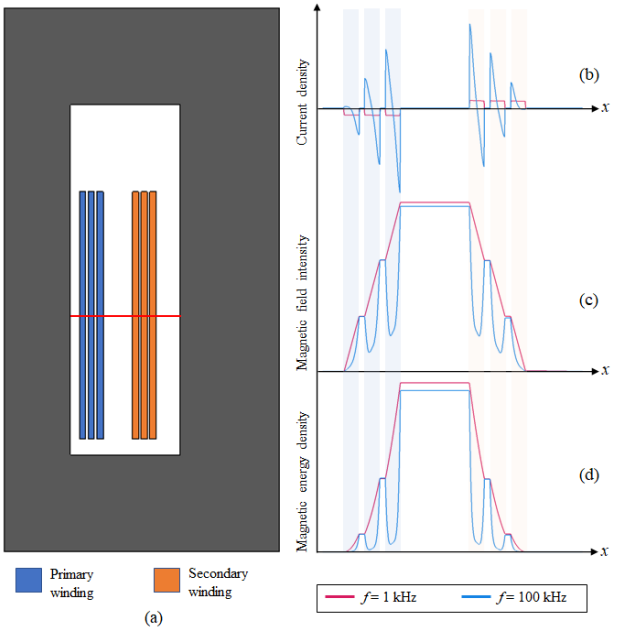

Fig. 4. (a) 2-D axisymmetric transformer cross-section with three primary and and three secondary winding layers. Corresponding FEM plots across the marked cut-line at different frequencies: (b) current density, (c) magnetic field intensity, (d) magnetic energy density.

IV. Dowell's 1-D Model

Fig. 4 shows a 2-D axisymmetric transformer cross-section with multiple rectangular foil layers that constitute the primary and secondary windings. It also shows the current density, magnetic field intensity and magnetic energy density plots at different frequencies across the marked cut-line, obtained from 2-D FEM simulations. At 1 kHz, the current density is uniform; so the corresponding change in magnetic field intensity is also linear across the foil cross-sections. But at 100 kHz, the skin and proximity effects cause a non-uniform current density that further lead to a non-linear magnetic field intensity across the foil cross-sections. These effects become more severe at higher frequencies as the skin depth δ shrinks further. δ is a measure of the current density across the cross-section of the conductor and is given by,

$$\delta = \sqrt{\frac{1}{\pi \mu f \sigma}} \tag{3}$$

where f is the frequency, and μ and σ are the permeability and conductivity of the material, respectively.

Fig. 4 further suggests that the skin and proximity effects influence the magnetic energy densities in the foil cross-sections only, but not so much in the non-winding spaces because the net current is conserved [14]. Hence, the winding cross-sections can be assumed as frequency-dependent regions and the non-winding spaces as frequency-independent regions. Dowell investigated the orthogonality between the two effects, and derived a simple 1-D model from Maxwell's equations.

Maxwell's equations for a divergence-free linear isotropic homogeneous medium with zero displacement current are,

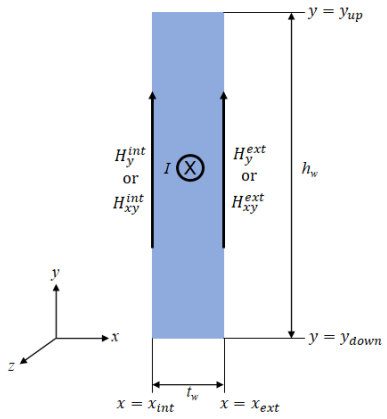

Fig. 5. Rectangular foil carrying a net current I.

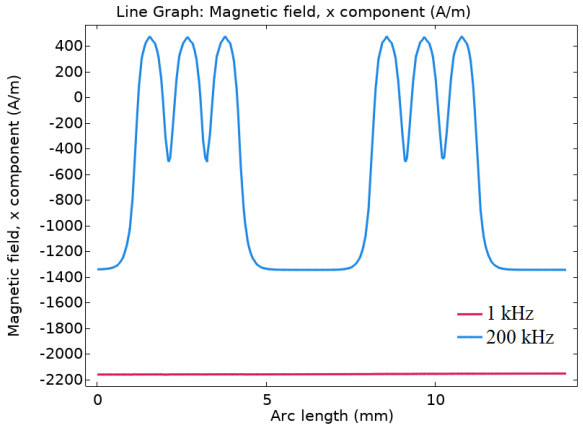

Fig. 6. H_x across a cut-line parallel to the $x-$axis and passing through the center of the IW plane when $g = 10.55$ mm.

$$\nabla \times E = -\mu_0 \cdot \frac{\partial H}{\partial t} \tag{4}$$

$$\nabla \times H = \sigma \cdot E. \tag{5}$$

For the rectangular foil in Fig. 5, assuming that the electric field intensity E has only the $z-$component and the magnetic field intensity H has only the $y-$component, E and H become functions of x only. Then, the Maxwell's equations in phasor form can be expressed as [14, 19],

$$\frac{dE_z}{dx} = j\omega\mu_0 H_y \tag{6}$$

$$\frac{dH_y}{dx} = \sigma E_z. \tag{7}$$

Using the above two equations, the Helmholtz second-order differential equation is reached below,

$$\frac{d^2 H_y}{dx^2} = j\omega\mu_0\sigma H_y. \tag{8}$$

The general solution of the Helmholtz equation is given by,

$$H_y(x) = H_1 e^{\gamma x} + H_2 e^{-\gamma x} \tag{9}$$

where γ is the propagation constant expressed as,

$$\gamma = \frac{1+j}{\delta} \tag{10}$$

and H_1 and H_2 are constants that can be obtained from the boundary conditions of the foil,

$$H_1 = \frac{H_y^{ext} e^{-\gamma x_{int}} - H_y^{int} e^{-\gamma x_{ext}}}{2\sinh(\gamma t_w)} \tag{11}$$

$$H_2 = \frac{H_y^{int} e^{\gamma x_{ext}} - H_y^{ext} e^{\gamma x_{int}}}{2\sinh(\gamma t_w)}. \tag{12}$$

Substituting H_1 and H_2 in (9) gives the frequency-dependent axial component of magnetic field intensity across the foil,

$$H_y(x) = H_y^{ext}\frac{\sinh(\gamma(x - x_{int}))}{\sinh(\gamma t_w)} + H_y^{int}\frac{\sinh(\gamma(x_{ext} - x))}{\sinh(\gamma t_w)} \tag{13}$$

Finally, the magnetic energy per unit area E''_{foil} across the foil can be evaluated,

$$E''_{\text{foil}} = \frac{\mu_0}{2}\int_{x_{int}}^{x_{ext}} H_y^2(x)\,dx. \tag{14}$$

The closed-form solution can be expressed as,

$$E''_{\text{foil}} = \frac{\mu_0\delta}{4}\left(\left(H_y^{ext} + H_y^{int}\right)^2\varphi_1 - 2H_y^{ext}H_y^{int}\varphi_2\right). \tag{15}$$

$$\varphi_1 = \frac{\sinh(2\Delta) - \sin(2\Delta)}{\cosh(2\Delta) - \cos(2\Delta)},\ \varphi_2 = \frac{\sinh(\Delta) - \sin(\Delta)}{\cosh(\Delta) - \cos(\Delta)}$$

where H_y^{int} and H_y^{ext} are the internal and external magnetic field intensities in $y-$direction evaluated at $x = int$ and $x = ext$ respectively, $\Delta = t_w/\delta$ is the penetration ratio, and t_w is the thickness of the foil. Here, φ_1 and φ_2 are the skin and proximity effect factors, respectively. To find the total magnetic energy across the foil, E''_{foil} in (15) must be scaled by the height h_w and the MLT d_w of the foil.

V. Hybrid Model

The semi-analytical hybrid model proposed in this paper is built on the double-2-D model platform presented in (2). It uses superposition to combine the HF Dowell's model with the LF double-2-D model. Dowell's model calculates the magnetic energy per unit length from the frequency-dependent winding cross-sections, while the double-2-D model calculates the same from the frequency-independent non-winding spaces.

Fig. 6 shows that H_x is non-negligible and varies along the $x-$axis at higher frequencies. Additionally, H_y varies along the height of the foil. To include the variations in H_x and H_y and to adhere to the double-2-D model requirements, Dowell's 1-D model in (15) is modified. For the same rectangular foil in Fig. 5, the modified Dowell's model evaluates the magnetic energy per unit length E'_{foil} across it using,

$$E'_{\text{foil}} = \frac{\mu_0\delta}{4}\int_{y_{down}}^{y_{up}}\left(\left(H_{xy}^{ext}(y) + H_{xy}^{int}(y)\right)^2\varphi_1 - 2H_{xy}^{ext}(y)H_{xy}^{int}(y)\varphi_2\right)dy \tag{16}$$

TABLE I
SPECIFICATIONS OF THE VIT

Turns ratio	1:1
Conductor type, size	Round, AWG 19
Number of turns per layer	30
Number of layers per winding	3
Core geometry	EC 70
Winding height	31.50 mm
External diameter of the movable bobbin	19 mm
External diameter of the fixed bobbin	33 mm
Insulation gap between layers	0.20 mm
Fill-factor	19.04 %
Maximum travel of the movable bobbin	11 mm
Test frequency range	1 – 200 kHz
Air cube (for OW plane boundary)	80^3 mm^3

where $H_{xy} = \sqrt{(H_x^2 + H_y^2)}$ accounts for the magnetic field intensities in both $x-$ and $y-$directions. Here, a similar treatment is given to both H_x and H_y in order to reduce the computational complexity. The integration in $y-$direction ensures the accurate estimation of the frequency-dependent magnetic energy per unit length across the foil. Besides, (16) also facilitates the use of partial leakage length as the depth of the plane under investigation.

$H_{xy}^{int}(y)$ and $H_{xy}^{ext}(y)$ in (16) are readily available from the double-2-D model by evaluating $H_x(x, y)$ and $H_y(x, y)$ at $x = int$ and $x = ext$, respectively. E'_{foil} is evaluated for each winding layer at the desired frequency. Since non-winding spaces are frequency-independent regions, the double-2-D model is directly used to compute the magnetic energy per unit length E'_{nw} across them, which remains constant at all frequencies. Using superposition, the net magnetic energy per unit length across a plane is obtained by summing the magnetic energies per unit length across all winding layers and non-winding spaces that constitute the plane, i.e. $E' = E'_{\text{foil(all)}} + E'_{\text{nw}}$. E' is scaled by a factor of $2/I_1^2$ to find the leakage inductance per unit length L' across the plane under investigation. Since a change in frequency barely changes the partial leakage lengths, they are directly obtained from the double-2-D model and remain constant at all frequencies. Finally, the leakage inductance of the transformer can be calculated by using,

$$L_{lk,\text{hybrid}} = s_c \left(L'_{(\text{IW})} d_{l(\text{IW})} + L'_{(\text{OW})} d_{l(\text{OW})}\right) \tag{17}$$

VI. RESULTS

Table I presents the specifications of the VIT pursued for validating the proposed hybrid model. MATLAB R2019a is used for all semi-analytical calculations considering the nearest two image layers in the IW plane. Fig. 7 shows the complete experimental setup with the VIT, linear actuator, 1 MHz LCR meter, and Arduino-based control circuitry. COMSOL Multiphysics 5.5 is used for obtaining the 2-D FEM results considered as standards for determining the errors. Figs. 8 and 9 plot the magnetic energy densities across the IW plane of the VIT at 1 and 200 kHz when $g = 0$ mm and $g = 11$ mm, respectively. A visual inspection between these plots suggests

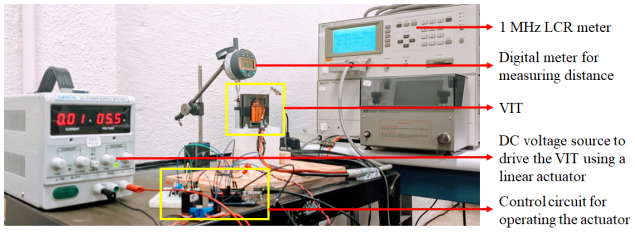

Fig. 7. Experimental measurement setup with the VIT.

the increase in leakage energy with g and its decrease with frequency. For the specific wire gauge, the frequency at which δ equals the radius of the conductor is 20.4 kHz.

Figs. 10, 11 and 12 compare the variations in the semi-analytically evaluated, FEM simulated and experimentally measured leakage inductances of the VIT with g at six different frequencies. These plots reiterates the fact that the effective leakage inductance of the VIT increases with g while decreases with frequency. In fact, the leakage inductance at $g = 11$ mm is nearly 80 % higher than that at $g = 0$ mm across all frequencies. The existing HF models cannot evaluate these variations in the frequency-dependent leakage inductance with g, resulting flat horizontal curve.

In all three figures, the FEM and the experimental curves nearly overlap each other at all frequencies. However, some errors can be observed between the FEM and the semi-analytical curves at higher g values, especially at 20, 30 and 50 kHz. One of the reasons for this discrepancy is the number of image layers being considered in the IW plane. By adding another layer, these errors can be reduced although the computation time may double because of twice as many images in the IW plane. Nevertheless, the maximum error is only 7.1 % observed at 50 kHz and $g = 11$ mm. Considering the challenging winding geometry of the VIT, this error is quite small. Therefore, it can be concurred that the proposed hybrid model can evaluate the variable HF leakage inductance of a VIT with sufficient accuracy. Between 1 and 200 kHz, the leakage inductance of the experimental prototype dropped by more than 18 % across all overlaps.

VII. CONCLUSION

This paper proposes a new hybrid model for evaluating the variable leakage inductance of a VIT at the desired frequency. This model uses superposition to combine the evergreen Dowell's model with the versatile double-2-D model. A modified Dowell's 1-D model calculates the leakage inductance contributions from the frequency-dependent winding cross-sections, while the double-2-D model calculates the same from the frequency-independent non-winding spaces. Using a 2-D model in the non-winding spaces and accounting for the actual positions of the windings make the hybrid model very attractive for any random winding geometry. The proposed model is validated through 2-D FEM simulations as well as experimental measurements. It can prove very effective in multi-objective optimization-based designs of power electronic converters employing transformers with integrated magnetics.

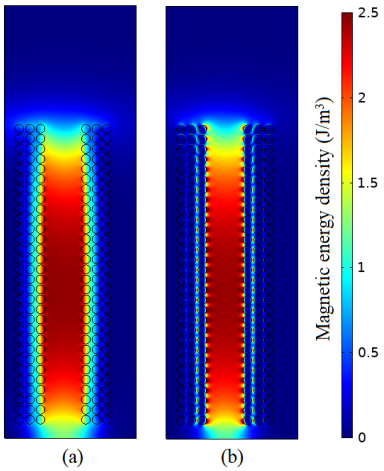

Fig. 8. Magnetic energy densities across the IW plane at $g = 0$ mm: (a) 1 kHz, and (b) 200 kHz.

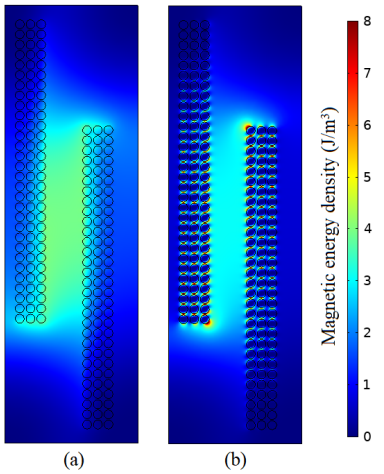

Fig. 9. Magnetic energy densities across the IW plane at $g = 11$ mm: (a) 1 kHz, and (b) 200 kHz.

VIII. Acknowledgements

This material is based upon work supported by the Department of Energy Vehicle Technologies Office under Award Number DE-EE0008449. This report was prepared as an account of work sponsored by an agency of the United States Government. Neither the United States Government nor any agency thereof, nor any of their employees, makes any warranty, express or implied, or assumes any legal liability or responsibility for the accuracy, completeness, or usefulness of any information, apparatus, product, or process disclosed, or represents that its use would not infringe privately owned rights. Reference herein to any specific commercial product, process, or service by trade name, trademark, manufacturer, or otherwise does not necessarily constitute or imply its endorsement, recommendation, or favoring by the United States Government or any agency thereof. The views and opinions of authors expressed herein do not necessarily state or reflect those of the United States Government or any agency thereof.

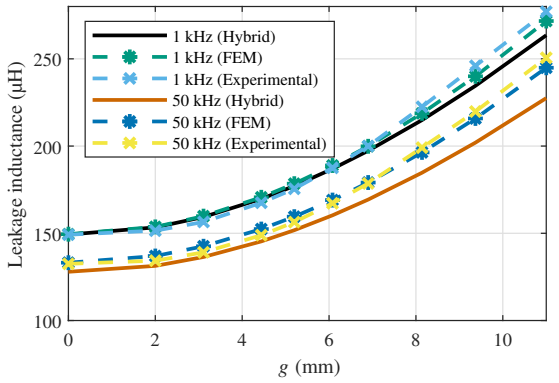

Fig. 10. Variation of leakage inductance with g at 1 and 50 kHz.

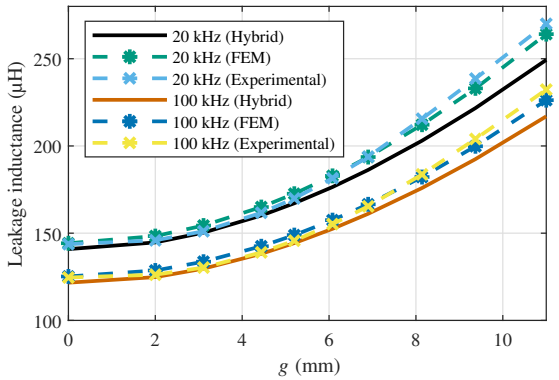

Fig. 11. Variation of leakage inductance with g at 20 and 100 kHz.

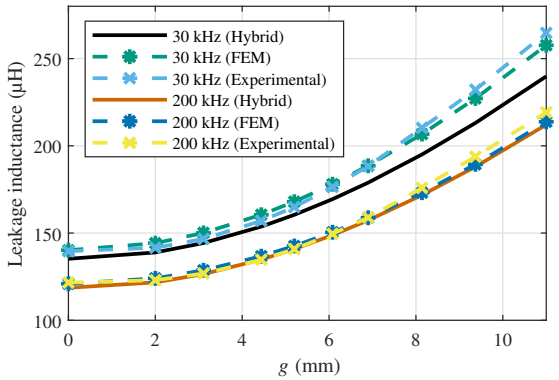

Fig. 12. Variation of leakage inductance with g at 30 and 200 kHz.

References

[1] M. Mogorovic and D. Dujic, "100 kw, 10 khz medium-frequency transformer design optimization and experimental verification," *IEEE Transactions on Power Electronics*, vol. 34, no. 2, pp. 1696–1708, 2019.

[2] A. Sharma and J. W. Kimball, "Evaluation of transformer leakage inductance using magnetic image method," *IEEE Transactions on Magnetics*, vol. 57, no. 11, pp. 1–12, 2021.

[3] A. Fouineau, M.-A. Raulet, B. Lefebvre, N. Burais, and F. Sixdenier, "Semi-analytical methods for calculation of leakage inductance and frequency-dependent resistance of windings in transformers," *IEEE Transactions on Magnetics*, vol. 54, no. 10, pp. 1–10, 2018.

[4] A. Garcia-Bediaga, I. Villar, A. Rujas, L. Mir, and A. Rufer, "Multi-objective optimization of medium-frequency transformers for isolated

soft-switching converters using a genetic algorithm," *IEEE Transactions on Power Electronics*, vol. 32, no. 4, pp. 2995–3006, 2017.

[5] R. Schlesinger and J. Biela, "Comparison of analytical models of transformer leakage inductance: Accuracy versus computational effort," *IEEE Transactions on Power Electronics*, vol. 36, no. 1, pp. 146–156, 2021.

[6] C. W. T. McLyman, *Transformer and inductor design handbook*. CRC press, 2004.

[7] P. Gomez and F. de León, "Accurate and efficient computation of the inductance matrix of transformer windings for the simulation of very fast transients," *IEEE Transactions on Power Delivery*, vol. 26, no. 3, pp. 1423–1431, 2011.

[8] M. Eslamian and B. Vahidi, "New methods for computation of the inductance matrix of transformer windings for very fast transients studies," *IEEE Transactions on Power Delivery*, vol. 27, no. 4, pp. 2326–2333, 2012.

[9] R. Prieto, J. Cobos, O. Garcia, P. Alou, and J. Uceda, "Study of 3-D magnetic components by means of "double 2-D" methodology," *IEEE Transactions on Industrial Electronics*, vol. 50, no. 1, pp. 183–192, 2003.

[10] V. S. Duppalli and S. Sudhoff, "Computationally efficient leakage inductance calculation for a high-frequency core-type transformer," in *2017 IEEE Electric Ship Technologies Symposium (ESTS)*, 2017, pp. 635–642.

[11] R. Schlesinger and J. Biela, "Leakage inductance modelling of transformers: Accurate and fast models to scale the leakage inductance per unit length," in *2020 22nd European Conference on Power Electronics and Applications (EPE'20 ECCE Europe)*, 2020, pp. P.1–P.11.

[12] A. Sharma and J. W. Kimball, "Novel transformer with variable leakage and magnetizing inductances," in *2021 IEEE Energy Conversion Congress and Exposition (ECCE)*, 2021, pp. 2155–2161.

[13] P. L. Dowell, "Effects of eddy currents in transformer windings," *Proceedings of the Institution of Electrical Engineers*, vol. 113, no. 8, p. 1387–1394, 1966.

[14] I. Villar, "Multiphysical characterization of medium-frequency power electronic transformers," Ph.D. dissertation, EPFL Lausanne, Switzerland, 2010.

[15] W. Hurley and D. Wilcox, "Calculation of leakage inductance in transformer windings," *IEEE Transactions on Power Electronics*, vol. 9, no. 1, pp. 121–126, 1994.

[16] D. Wilcox, M. Conlon, and W. Hurley, "Calculation of self and mutual impedances for coils on ferromagnetic cores," *IEE Proceedings A-Physical Science, Measurement and Instrumentation, Management and Education-Reviews*, vol. 135, no. 7, pp. 470–476, 1988.

[17] V. Niemela, G. Skutt, A. Urling, Y.-N. Chang, T. Wilson, H. Owen, and R. Wong, "Calculating the short-circuit impedances of a multiwinding transformer from its geometry," in *20th Annual IEEE Power Electronics Specialists Conference*, 1989, pp. 607–617 vol.2.

[18] M. A. Bahmani and T. Thiringer, "Accurate evaluation of leakage inductance in high-frequency transformers using an improved frequency-dependent expression," *IEEE Transactions on Power Electronics*, vol. 30, no. 10, pp. 5738–5745, 2015.

[19] Z. Ouyang, J. Zhang, and W. G. Hurley, "Calculation of leakage inductance for high-frequency transformers," *IEEE Transactions on Power Electronics*, vol. 30, no. 10, pp. 5769–5775, 2015.

[20] M. Mogorovic and D. Dujic, "Medium frequency transformer leakage inductance modeling and experimental verification," in *2017 IEEE Energy Conversion Congress and Exposition (ECCE)*, 2017, pp. 419–424.